34th Annual International Conference of the IEEE EMBS
San Diego, California USA, 28 August - 1 September, 2012

Design of a Two Degree-of-Freedom, MRI-Compatible Actuator*

Khaled M. Elbannan and Shaun P. Salisbury, *Member, IEEE*

***Abstract*—A novel compact piezoworm actuator for the MRI (Magnetic Resonance Imaging) environment is presented which is capable of both linear and rotary motion. The actuator will be fabricated from beryllium copper for minimal image distortion. Complementary clamps are integrated to minimize the number of drive channels and to act as a brake in case of a malfunction. Analysis was employed to optimize the selection of the piezostacks and flexures depending on their functional requirements. The device is targeting a maximum speed of 5 mm/s, a force thrust of 9 N and 5 rpm of rotational speed.**

I. Introduction

MRI (Magnetic Resonance imaging) has become a standard diagnostic tool in hospitals around the world and is increasingly used in performing image-guided intervention (IGI) procedures. The trend of using remotely actuated and controlled devices to assist in the performance of MRI-guided interventions are increasing [1] since its image quality is superior to other modalities. Brachytherapy and biopsy medical procedures can be conducted using MRI-guided interventional technology for accurate navigation of the needle. The main goal is to insert the needle with high accuracy resulting in a more effective treatment [2]. The key point of accurate placement is rotating the needle round its own axis either using continuous spinning or pulsation methods [2-5]. This emphasizes the need for a two degree-of-freedom actuator for this type of MRI-guided medical procedures.

Despite all the advantages of MRI, the extreme magnetic fields (up to 7 Tesla), rapidly changing magnetic field gradients (GR), and radiofrequency (RF) pulses used in operating the scanner [6] make it a difficult environment in which to operate actuators. One must consider the induced forces and torques and image distortion caused by the introduction of the device into the MR scanner. Heating of the device may also be a concern. Heating results from the interaction of the device with the RF magnetic field and/or the switching gradient fields which can be create eddy currents, induction loops, or resonating RF waves along conductors as discussed in [7-9]. Additionally, the limited space inside MRI scanner bore necessitates a compact actuator so the materials employed must be strong and rigid as well being MR-compatible [1,6,10,11].

Several designs of actuators for MR-compatible applications have been developed. Hydraulic actuation is a stiff MR-compatible method of actuation as described in [12] but it is difficult to control and requires heavy infrastructure. Pneumatic methods of actuation are low cost, compact in size, and posses a high power-to-weight ratio as in the case of PneuStep [13], but low stiffness and performance degradation with time are some of its disadvantages. If remote actuation is considered as in [14] this will drastically decrease the stiffness of the system, as remote systems suffer from joint flexibility, backlash, and friction. Manual actuation is a simple method of actuation as in the MRI guided needle interventions in [15]. The major drawback in this case is large device size.

One of the commonly utilized technologies for MR-compatible actuators has been piezoelectric motors. In [16], a rotary-linear piezoelectric actuator was developed based on ultrasonic motors using three vibration modes. It was a very compact design however its thrust force was below 0.5 N. In this paper, the piezoelectric actuation method is also employed but it will be used in a piezoworm-type (also called inchworm®) actuator which combines three or more piezostacks [17]. This retains attractive features like the high positioning resolution, high stiffness and MRI compatibility but has much higher output force.

To establish appropriate performance targets we considered the research on needle insertion in skin and soft tissues presented in [2-5]. Testing done in [2] simulated the needle forces using 18 gauge needle inserted in a soft material phantom from polyvinylchloride (PVC). Tests were done at different insertion and rotational speeds and resulted in a maximum insertion force of almost 9 N and torque of 1.6 N.mm. Using these results as the basis for a common needle-guided intervention we targeted an actuator with a 50 mm range, linear speed up to 5 mm/s, rotary speed of 5 rpm, output thrust up to 9 N and a torque exceeding 2 N.mm.

The concept and design parameters of the novel piezoworm motor are presented in the following sections. Section II describes the actuation principle with the complementary clamp arrangements. Section III then presents the actuator design and the analysis performed. The conclusions are summarized in Section IV.

II. Actuation Principle

The proposed actuator design is shown in Fig. 1. It is based on the piezoworm configuration which employs two piezostacks to clamp the shaft and a third piezostack to provide the linear motion. The same set of clamps is used for both linear and rotary motion. A fourth piezostack was added which rotates the plate attached to the front clamp to get the rotary motion. By using the same set of clamps for both linear and rotary motion the overall size of the actuator is reduced. By using separate actuators for each degree-of-freedom the motions can be undertaken separately or jointly

*Research supported by the Natural Sciences and Engineering Research Council of Canada.

S. P. Salisbury is with the Department of Mechanical & Materials Engineering, University of Western Ontario, 1151 Richmond Street, London, Ontario, Canada, N6A 5B9. (Phone: 519-661-2111, Fax: 519-661-3020, E-mail: ssalisb2@uwo.ca)

K. M. Elbannan is with Department of Mechanical & Materials Engineering, University of Western Ontario, 1151 Richmond Street, London, Ontario, Canada, N6A 5B9. (E-mail: kelbanna@uwo.ca).

to achieve the required motion. The piezostacks are preloaded by setscrews to keep them always in compression to prevent damage from tensile forces. Utilizing a shaft as the moving member, similar to [18], minimizes the size (and its MRI signature) but reduces the thrust capacity as compared to piezoworms that run inside a channel [19]. In future refinements of this design we hope to act directly on the needle during the intervention but at this time we are planning to integrate it into the shaft for our testing.

The clamp arrangement is based on the complementary clamp concept developed in [20]. One clamp is designed to grip the shaft when the piezostack is energized and is designated the normally unclamped (NU) clamp. The other clamp is designated as normally clamped (NC) and grips the shaft when the piezostack is de-energized. The advantage of this arrangement is that in a conventional piezoworm [21] complete steps are done in six successive actuation operations but in the case of a complementary piezoworm only four actuation operations are required (see Fig. 2) [20]. This is because both clamps are fed from one signal amplifier, so one clamp opens and the other closes during the same time frame. Delay circuits can be used [20] to increase the force during the transition of the clamps. Another important benefit of using complementary clamps is that if the power is suddenly lost the shaft will automatically be secured safely in place.

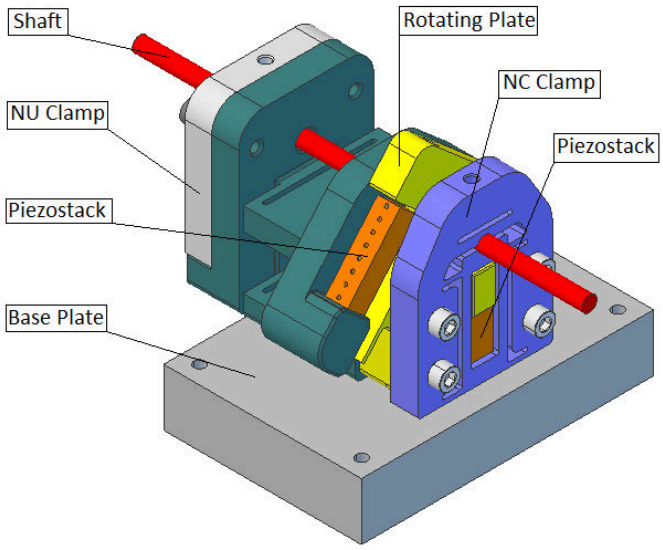

Figure 1: Actuator model.

To achieve the rotary motion the NC clamp has been mounted on a plate which can rotate about the axis of the shaft. A piezostack drives the rotary motion against a flexure machined into the rotary plate which returns the plate to its original orientation when the piezostack is de-energized. The piezostack is also preloaded with a setscrew. The speed of the linear and rotary motion can be controlled by both the amplitude and the frequency of their voltage waveforms. The direction of motion is dictated by the sequence of the actuation operations.

III. Actuator Design

The challenging environment and available space inside the MRI scanner require the actuator design to strike a balance between several competing objectives. Good thrust and torque, long linear travel range, and high stiffness are the design main performance objectives while minimizing size and image distortion. The range of travel for the proposed actuator is limited only by the available space inside the scanner. The available space depends on orientation of the actuator in the MR scanner bore as well as the part of the body being imaged.

Selecting suitable material for the MR-compatible actuator is a challenging task as various parameters come into play such as susceptibility, resistivity, strength, and stiffness of material as discussed in [22]. The principal material property affecting image distortion is the material susceptibility. It also dictates the magnitudes of the forces and torques acting on the actuator. The material selection criterion for the proposed device was based on minimizing the susceptibility and maximizing the stiffness and strength. Hardened beryllium copper (UNS C17510) was chosen as an optimal material for this task as it strikes a balance between high stiffness and low susceptibility when compared to other engineering material tested in [22]. Though beryllium copper is expected to show some rise in temperature as presented in [7] this can be compensated by insulating the interface between the medical tool and the actuator for maximum patient safety.

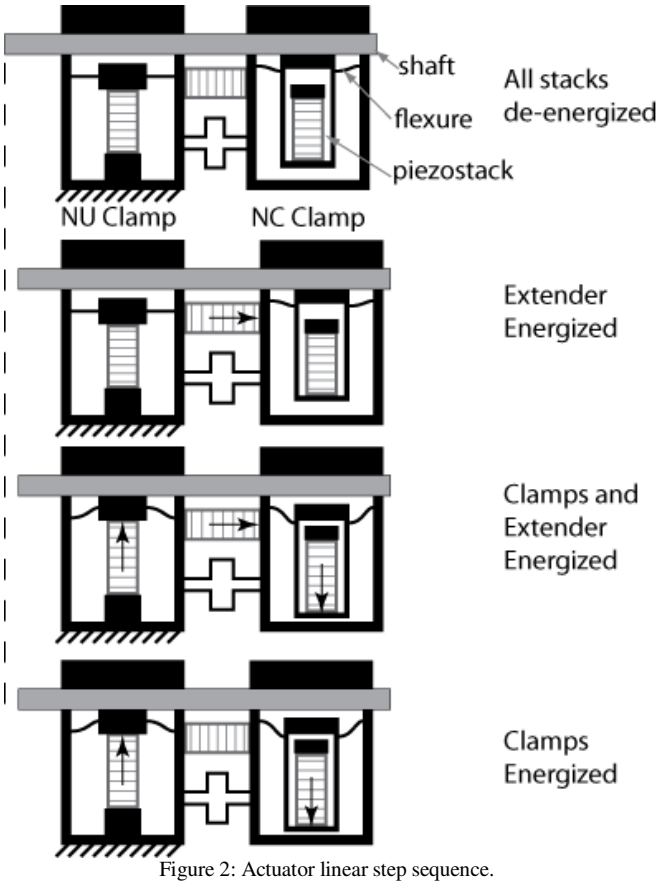

Figure 2: Actuator linear step sequence.

A. *Extension frame design*

Maximizing the speeds (linear and rotary) while minimizing the size of the actuator is critical for maneuvering tools inside the limited space inside the MRI scanner and decreasing the duration of the medical procedure. The critical factors in the speed of the actuator are the displacement range of the extender frame shown in Fig. 3 and its resonant frequency. To maximize the speed the design of the flexure must be designed to maximize the piezostack expansion but it must be such that the resonant frequency is larger than the operating frequency. The constrained expansion of the piezostack, Δ, is given by (1) where k_p is the piezostack stiffness k_f is the flexure stiffness and Δ_0 is the free expansion of the piezostack.

$$\Delta = \frac{k_p}{k_p + k_f}\Delta_0 \quad (1)$$

A piezostack, Physik Instrumente (PI) P-885.51, was selected which is 5 mm by 5 mm in cross section and has a length of 18mm. Its nominal displacement is 15 µm at 100 V and has a stiffness of 50 N/µm. The length and thickness of the flexure were set to 6 mm, 1.5 mm respectively to give a resonant frequency of 1574 Hz. The total effective stiffness of the flexures was 16.1 N/µm. When considering the frame stiffness, the frame will have an expansion of 11 µm based on calculation presented in [20]. The maximum speed of the motor is expected to be about 9 mm/s based on a driving frequency of 800 Hz.

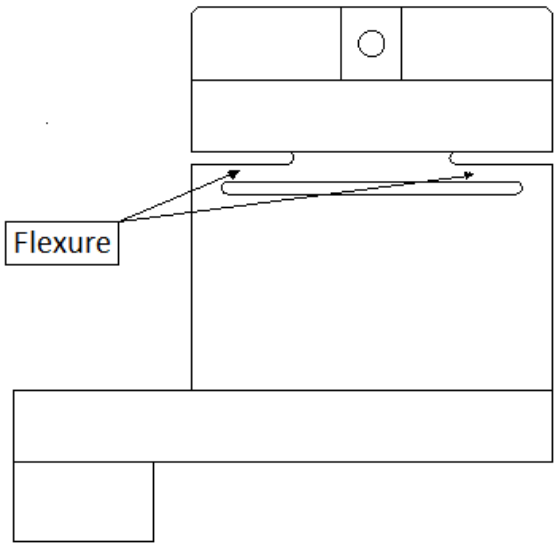

Figure 3: Extension frame.

B. *Rotation frame design*

Similar to the extension frame, the rotational speed is affected by the displacement range of the piezostack and the resonant frequency. But this frame (Fig. 4) has an additional factor which is the distance away from the center of rotation. With a fixed piezostack displacement, increasing the arm of rotation will result of larger torque and lower speed. On the contrary, decreasing the arm will result in higher speed and lower torque. The arm length was selected to be 11.75 mm to optimize for maximum speed at the targeted torque. The rotating plate flexure width is 6 mm and its length and thickness were set to 6.5 mm and 0.8 mm respectively to give a resonant frequency of 5928 Hz. The stiffness of the flexure is 1.6 N/µm. Based on (1), the frame will have an expansion of 12 µm. The maximum speed of the motor is expected to be about 8.5 rpm and torque of at least 5 N.mm based on a driving frequency of 800 Hz.

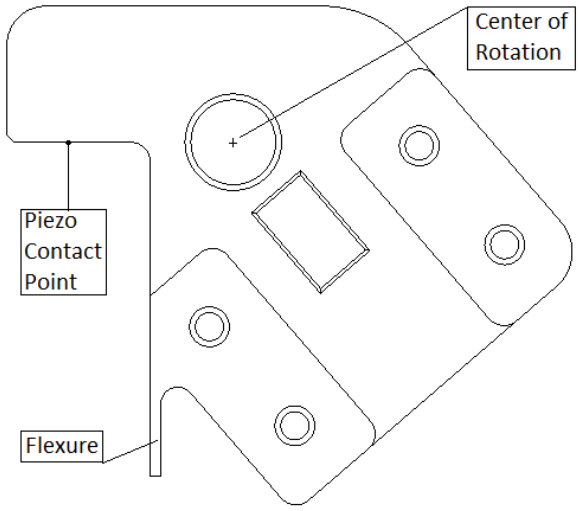

Figure 4: Rotation frame.

C. *Clamp Design*

The clamp configurations are shown in Fig. 5 and 6 in both their energized and de-energized states. The piezostack shown in gray pushes against the black tab which is rigidly fixed to the supporting frame. The displacements shown are exaggerated for clarity as the actual displacements are in micrometers.

In [17], it was thought that ideally both clamps should be the same shape and size to perform a fully complementary action, so as to achieve the same dynamic performance and to facilitate simultaneous manufacturing using electro-discharge machining. However, the way in which each clamp develops its clamping force is different. In the NU clamp, the piezostack pushes up to grip the shaft so the flexure in this case is simply to guide and protect the piezostack. The NU flexure stiffness should be minimized so as to not impede the piezostack motion and will in turn increase its clamping force. The lower bound on the flexure stiffness is governed by the maximum bending stress.

The NC clamp grips the shaft when it is de-energized so the clamp force is developed by the displacement of its flexure. Now, the flexure stiffness must be maximized in order to get the most clamping force. However, if the flexure is too stiff the piezostack will not be able to fully disengage the clamp. Bending stress is also a consideration here as well.

Both clamps use the same ceramic material piezostack element from PI, P-885.11. The piezostacks have a cross section of 5 mm by 5mm and a length of 9 mm. Their nominal displacement is 6.5 µm at 100 V with a stiffness of 100 N/µm. These piezostacks were selected for this application as they offer high stiffness in small size package,

and sufficient nominal displacement. The flexure width and thickness were set at 6 mm and 1 mm respectively. The length of the flexures was varied to achieve the desired stiffness for each type of clamp. The NU flexure has a length of 4 mm which gives a stiffness of 19.5 N/µm, and the NC flexure is 5 mm long with a stiffness of 10.6 N/µm. The predicted clamp forces are 43 N for the NU and 34 N for the NC clamp. The resonant frequency is 18243 Hz for the NU clamp and 7370 Hz for the NC clamp which is well above the maximum drive frequency of 800 Hz.

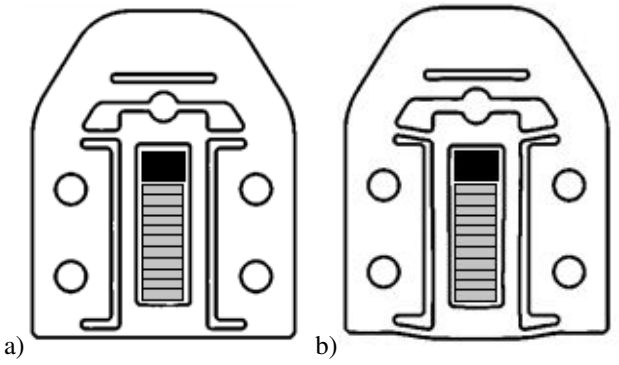

Figure 5: NC clamp a) de-energized, b) energized.

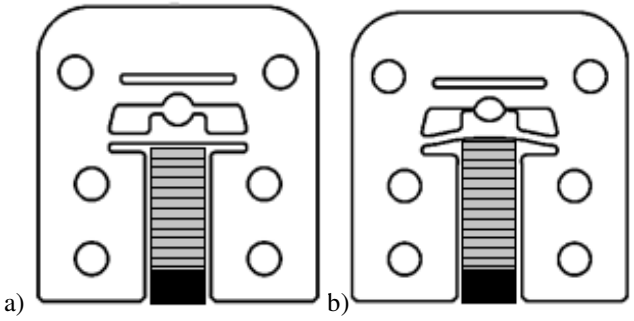

Figure 6: NU clamp a) de-energized, b) energized.

IV. CONCLUSIONS

A novel two degree of freedom piezoworm actuator was developed specifically to be MR-compatible. Rotational and linear motions can be actuated simultaneously or separately according to the demands of the medical procedure. The structural elements are made from beryllium copper and the clamps are configured as complementary clamps for maximum performance and safety. The design calculations showed that the performance targets should be achieved in the compact envelope. Prototype construction and experimental evaluation will be conducted to verify the actuator's performance. Then it will be tested in an MR scanner to confirm its compatibility.

REFERENCES

[1] N. V. Tsekos, A. Khanicheh, E. Christoforou, and C. Mavroidis, "Magnetic resonance–compatible robotic and mechatronics systems for image-guided interventions and rehabilitation: a review study," *Annu. Rev. Biomed. Eng.*, vol. 9, 2007, pp. 351-387

[2] T. K. Podder, D. P. Clark, D. Fuller, J. Sherman, W. S. Ng, L. Liao, D. J. Rubens, J. G. Strang, E. M. Messing, Y. D. Zhang, and Y. Yu, "Effects of velocity modulation during surgical needle insertion", *Proceedings of the 2005 IEEE Engineering in Medicine and Biology 27th Annual Conference*, Shanghai, China, September 1-4, 2005, pp/ 5766-5770.

[3] N. Abolhassani1, R. Patel, and F. Ayazi, "Effects of different insertion methods on reducing needle deflection," *Proceedings of the 29th Annual International Conference of the IEEE EMBS*, Lyon, France, August 23-26, 2007, pp. 491-494.

[4] N. Abolhassani, R. Patel, M. Moallem, "Needle insertion into soft tissue: A survey," *Medical Engineering & Physics* vol. 29, 2007, pp. 413–431.

[5] N. Abolhassani, R. Patel, F. Ayazi, "Needle control along desired tracks in robotic prostate brachytherapy," *IEEE International Conference on Systems Man and Cybernetics*, 2007, pp. 3361-3366.

[6] N. Yu, R. Riener, "Review on MR-compatible robotic systems," *IEEE/RAS-EMBS International Conference on Biomedical Robotics and Biomechatronics,* 2006, pp. 661-665.

[7] H. Graf, G. Steidle, and F. Schick, "Heating of metallic implants and instruments induced by gradient switching in a 1.5-tesla whole-body unit," *Journal of Magnetic Resonance Imaging*, vol. 26, 2007, pp. 1328–1333.

[8] M. K. Konings, L. W. Bartels, H. F. M. Smits, and C. J. G. Bakker, "Heating around intravascular guidewires by resonating RF waves", *Journal of Magnetic Resonance Imaging*, vol. 12, 2000, pp. 79–85.

[9] R. Buchli, P. Boesiger, D. Meier, "Heating effects of metallic implants by MRI examinations," *Magnetic Resonance in Medicine*, vol. 7, 1988, pp. 255–261.

[10] J. F. Schenck, "Invited safety of strong, static magnetic fields," *Journal of Magnetic Resonance Imaging*, vol. 12, 2000, pp. 2–19.

[11] K. Chinzei, R. Kikinis, and F.A. Jolesz, "MR compatibility of mechatronic devices: design criteria," *Int. Conf Med Image Computer Assist. Interv.*, 1999, pp. 1020-1031.

[12] R. Moser, R. Gassert, E. Burdet, L. Sache, H.R. Woodtli, et al, "An MR compatible robot technology," *Proc. IEEE Int. Conf. Robotics Automation*, Taipei, Taiwan, 2003, pp. 670–675.

[13] D. Stoianovici, A. Patriciu, D. Mazilu and L. Kavoussi, "A new type of motor: pneumatic step motor", *IEEE/ASME Transaction on Mechatronics*, vol. 12, 2007, pp. 98-106.

[14] E. Christoforou and N.V. Tsekos, "Robotic manipulators with remotely actuated joints: implementation using drive shafts and u-joints," *Proc. IEEE Int. Conf. Robotics Automation*, Orlando, FL, 2006, pp. 2886–2871.

[15] Krieger et al, "Design of a novel MRI compatible manipulator for image guided prostate interventions", *IEEE Transaction on Biomedical Engineering*, vol. 52, 2005, pp. 306-313.

[16] T. Mashimo, S. Toyama, and H. Matsuda, "Development of rotary-linear piezoelectric actuator for MRI compatible manipulator", *IEEE/RSJ International Conference on Intelligent Robots and Systems*, Nice, France, 2008, pp. 22-26.

[17] S. Salisbury, R. Ben Mrad, D. Waechter and S. Prasad, "Design, modeling and closed loop control of a complementary clamp piezoworm actuator," *IEEE/ASME Transactions on Mechatronics*, vol. 14, no. 6, 2009, pp. 724-732.

[18] W. May Jr., "Piezoelectric electromechanical translation apparatus," US Patent 3 902 084, Aug. 26, 1975.

[19] P. E. Tenzer and R. Ben Mrad, "A systematic procedure for the design of piezoelectric inchworm precision positioners", *IEEE/ASME Transactions on Mechatronics*, vol. 9, 2004, pp. 427-435.

[20] S. Salisbury, D. F. Waechter, R. Ben Mrad, S. E. Prasad, R. G. Blacow, and B. Yan, "Design considerations for complementary inchworm actuators," *IEEE/ASME Trans. on Mechatronics*, vol. 11, no. 3, 2006, pp. 265-272.

[21] B. Zhang and Z. Zhu, "Developing a linear piezomotor with nanometer resolution and high stiffness," *IEEE/ASME Transactions on Mechatronics*, vol. 2, no. 1, Mar. 1997, pp. 22-29.

[22] K. Elbannan, W. Handler, C. Wyenberg, B. Chronik and S. P. Salisbury, "Prediction of force and image artifacts under MRI for metals used in medical devices," *IEEE/ASME Transactions on Mechatronics*, 2012, in review.